

Biophysical Journal, Volume 97

Supporting Material

Elucidating the mechanism behind irreversible deformation of viral capsids

Anton Arkhipov, Wouter H Roos, Gijs J.L. Wuite, and Klaus Schulten

Supporting Material

1 Supporting Movies

- **Movie 1** shows a shape-based coarse-grained (SBCG) simulation with three rounds of AFM nanoindentations for $Z_{max} = 0.35R$ (the last round is continued up to $Z_{max} = 1.25R$).
- **Movie 2** shows an SBCG simulation with three rounds of AFM nanoindentations for $Z_{max} = 1.25R$.

2 Supporting Methods

Parameterization of bonded interactions

Parameters for bonded interactions (K_i , L_i , M_k , and Θ_k in Eq. 1 of the main text) are obtained from an all-atom simulation of an HBV capsid monomer in water, using the Boltzmann inversion method. The Boltzmann inversion for harmonic potentials estimates the CG parameters using the average of the bond length (angle) and its root mean square deviation (RMSD) obtained from the all-atom simulation (1–4):

$$\begin{aligned} L_i^{BI} &= \langle R_i \rangle, \\ K_i^{BI} &= \frac{k_B T}{2(\langle R_i^2 \rangle - \langle R_i \rangle^2)}, \\ \Theta_k^{BI} &= \langle \theta_k \rangle, \\ M_k^{BI} &= \frac{k_B T}{2(\langle \theta_k^2 \rangle - \langle \theta_k \rangle^2)}, \end{aligned} \tag{S1}$$

where k_B is the Boltzmann constant, T is the temperature, and $\langle \dots \rangle$ designates averaging over the simulation. The superscript “BI” stands for “Boltzmann inversion”.

After using the Boltzmann inversion result as an initial guess for the parameters of the SBCG model, we scale those parameters uniformly over i and k until the stiffness of the SBCG model matches that of the all-atom model (3) (see Fig. S1). The comparison is between the all-atom simulations of an HBV monomer and the SBCG simulation of the same monomer. In Fig. S1, the results of the Boltzmann inversion for the all-atom simulation and two SBCG simulations are shown, being reported as L_i^{BI} , Θ_k^{BI} , K_i^{BI} , and M_k^{BI} obtained through Eqs. S1. As such, these results correspond to the average (over simulated time) bond lengths, angles, and bond and angle RMSDs, respectively, i.e., they characterize the local stiffness of the protein. The first SBCG simulation (red) uses the parameters from the Boltzmann inversion of the all-atom simulation, but one finds that in this CG simulation the angles in the monomer model are too stiff. The second SBCG simulation (cyan) uses the same parameters as the first one but for the angle force constants, which are uniformly scaled by 0.3. As a result, the monomer stiffness in the second SBCG simulation is close to that in the all-atom simulation, and therefore the second set of the bonded parameters is used for all further SBCG simulations.

The inter-monomer bonds are assigned the L_i values based on the distances between the corresponding bead sites in the native capsid structure, and K_i values are chosen as averages of the K_i values for the monomer.

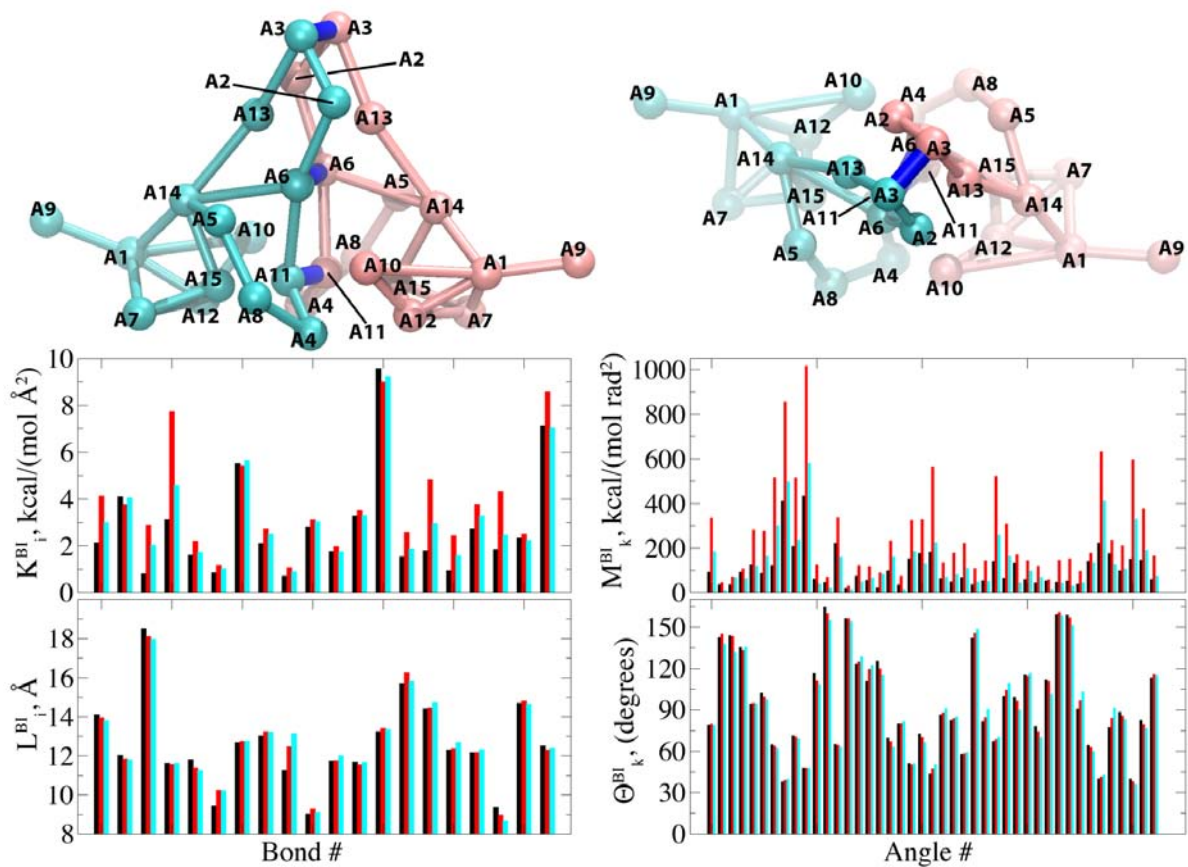


Figure S1: SBCG model of an HBV capsid protein. Two monomers forming a dimer are shown. Each monomer consists of 15 CG beads, named A1 to A15. Tuning of parameters for bonded interactions is illustrated here. The parameters plotted are obtained from all-atom and CG simulations of a monomer using Boltzmann inversion, i.e., the parameters characterize the average bond lengths and angles, as well as their RMSD, as recorded in the respective simulations. Black, all-atom simulation; red, SBCG simulation with parameters obtained using the Boltzmann inversion from the all-atom simulation; cyan, SBCG simulation with scaled parameters.

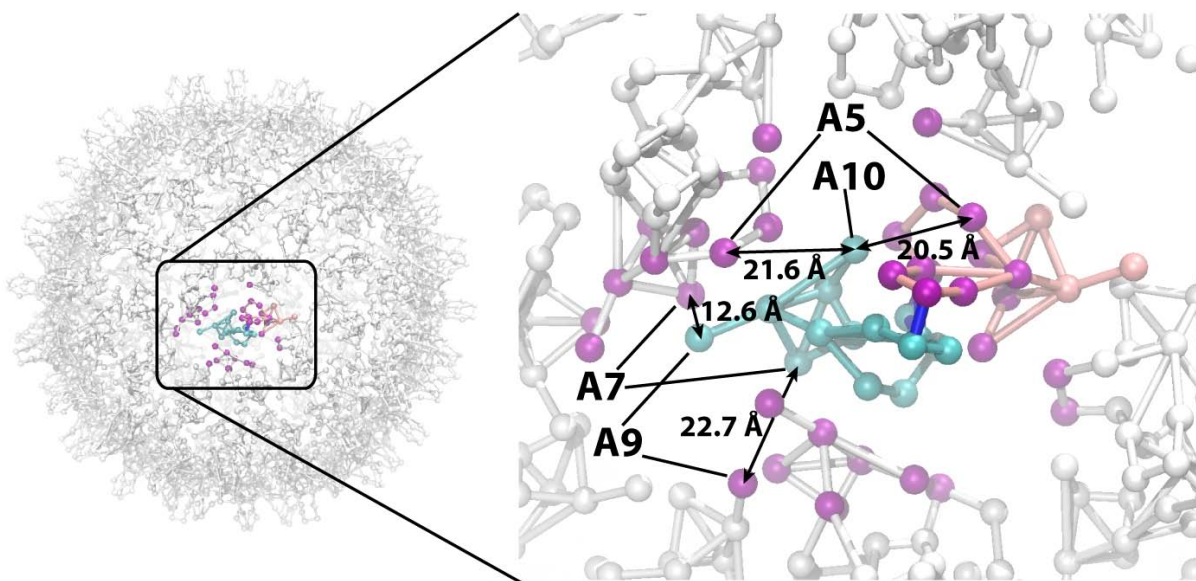


Figure S2: Choice of LJ interactions for the SBCG model of the HBV capsid. Two monomers (cyan and pink) forming a dimer are shown. All beads within 24 Å from the cyan monomer are highlighted in purple. Bead pairs A5-A10 and A7-A9 exemplify cases for which unique LJ interaction radii σ_{mn} can or cannot be set, respectively. For all possible A5-A10 pairs, the distances between beads A5 and A10 from different monomers within the 24 Å cutoff are close to each other (20.5 or 21.6 Å), and a single value of σ_{mn} can be chosen to describe these distances approximately. Note that the example shown here is for one monomer only. The actual LJ parameters are chosen based on the analysis of the whole T=4 capsid structure, where monomers are found in four non-equivalent orientations. Then, one finds that for the pairs A5-A10 a distance of 16.5 Å occurs with the same frequency as 20.5 and 21.6 Å, and σ_{mn} is set to the average, 19.5 Å. For A7-A9 pairs, the distances one finds are far off from each other, namely, 12.6 and 22.7 Å. Therefore, a specific LJ interaction between beads A7 and A9 is not established.

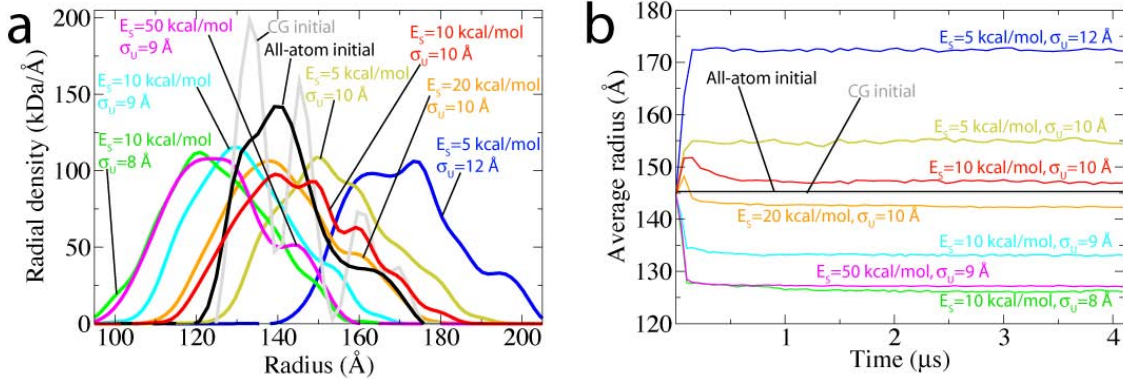


Figure S3: SBCG simulations of an HBV capsid with various values of the LJ parameters. Shown are several examples from the set of sampled parameter values; the sampled parameters are the LJ energy of specific interactions E_S and the uniform LJ radius of non-specific interactions σ_U . The simulated system contains only the capsid and ions, but no substrate or AFM tip. **a**, Radial density of the capsid at the end of simulations. **b**, Average radius of the capsid as a function of time in each simulation. Black and gray curves correspond to the properties computed for the all-atom native capsid structure and for the SBCG model of that structure, respectively. In **b**, the black and gray lines designate the average radii for the respective static structures.

Non-bonded interactions

Once the bonded parameters for the SBCG monomer model have been tuned, we consider the non-bonded parameters, which have the strongest influence on the shape and size of the HBV capsid. The non-bonded parameters (Eq. 1 of the main text) are charges q_m , dielectric constant ϵ , and LJ parameters ϵ_{mn} and σ_{mn} for bead pairs m - n . The tuning is done by running multiple SBCG simulations of a complete capsid (without the substrate and AFM tip) with different sets of the non-bonded parameters values, and comparing the size and mass distribution of the capsid in the simulations to those of the native capsid (the latter is known to be stable).

The dielectric constant ϵ should be 80 for bulk water and 1 for direct unscreened electrostatic interactions; either of the two values, and some in between, have been used in previous applications of SBCG and other CG models (1–8). For the tuning simulations of HBV capsid, we have tried the value of ϵ to be set to 1 or 15, as well as setting all charges to 0, together with varying the LJ parameters as described below. Either setting of the electrostatic interactions have been found to result in approximately the same behavior of the SBCG capsid, from which we conclude that the large-scale electrostatic interactions are not important for this system, as compared to the SBCG LJ interactions (the latter strongly influence the behavior of the capsid, as we discuss below). Therefore, we have chosen to use an intermediate value of $\epsilon = 15$ for our subsequent SBCG simulations.

Tuning the LJ parameters ϵ_{mn} and σ_{mn} has proven to be the most difficult and crucial part of the SBCG parameterization. In previous SBCG applications (3, 4), these parameters for a pair of beads m and n were approximated as $\epsilon_{mn} = \sqrt{\epsilon_m \epsilon_n}$, and $\sigma_{mn} = 0.5(\sigma_m + \sigma_n)$, which is a common choice for all-atom simulations. Here, ϵ_m and σ_m are the parameters for individual beads, the first being set based on the amount of the hydrophobic solvent-accessible surface area of the Voronoi cell of the bead, and the second based on the Voronoi cell’s gyration radius. However, interactions between all monomers in the HBV capsid structure have proven to be very specific, as the dimers forming the capsid are rather sparsely connected through precisely positioned salt bridges and clusters of overlapping hydrophobic residues, mainly around the 3-fold and 2-fold symmetry axes of the capsid (9). Fig. 1b in the main text shows that in the SBCG representation the inter-monomer contacts are indeed loose. The approach for setting the LJ parameters as described above has been unsuccessful in maintaining the correct capsid size and mass distribution in SBCG simulations. After trying 15 simulations with different maximal strengths for ϵ_m and different additions to the gyration radius in obtaining σ_m , it became clear that such SBCG model lacks enough specificity to maintain the appropriate capsid geometry.

Thus, we assigned the LJ parameters for specific pairs of the CG beads, depending on the distance between the two beads within the pair in the native capsid. The choice of such interactions is illustrated in Fig. S2. Since the capsid is composed of 240 identical monomers, each consisting of the same 15 beads, it is impossible to specify interactions between each bead in every monomer with each bead in every other monomer. This approach would be also impractical, as $\sim 3,600^2/2$ interactions would have to be specified, and most of them would be very far-range, making the force-field highly artificial.

Instead, we consider first all beads in the native capsid that are within a certain cutoff distance from any bead of a given name, e.g., A5 (see Fig. S2). The average gyration radius of the protein piece represented by a CG bead is 6 \AA , corresponding to the bead “size” of $S = 12 \text{ \AA}$, while the common cutoff distance in all-atom simulations is $R_{AA}^{cutoff} = 12 \text{ \AA}$ or less; thus, the cutoff distance for choosing the beads is set to $R_{CG}^{cutoff} = S + R_{AA}^{cutoff}$, or 24 \AA . For each pair of bead types that are closer than 24 \AA (e.g., A5 and A10 in Fig. S2) we consider all possible distances occurring in the native capsid. The distances within one monomer are not taken into account, since the interactions within the monomer are dominated by the bonded terms. For some pairs, several distances that are quite widely distributed are found, such as 12.6 and 22.7 \AA for the pair A7-A9 in Fig. S2. No specific interactions are assigned to those bead pairs. For others, all distances found fall within a tight range, e.g., distances of 16.5 , 20.5 , and 21.6 \AA occur with the same frequency for the pair A5-A10. According to the average radius of a CG bead, 6 \AA , we consider all the distances to fall within a “close range” if they are all within 6 \AA from each other. In such case, a specific LJ interaction is assigned to the pair $m - n$, with parameters $\epsilon_{mn} = E_S$ (where the “specific interaction energy” E_S is a constant, uniformly set up for all such specific interactions), and σ_{mn} is set to the average of the distances found for the

pair. Eleven such pairs of bead types have been identified, and specific interactions have been assigned for them. For all other pairs, we set LJ interactions to be non-specific, namely, $\epsilon_{mn} = 0.01$ kcal/mol and $\sigma_{mn} = \sigma_U$, where the uniform non-specific interaction radius σ_U is the same for all pairs. With such settings, for example, the interaction parameters for the pair A5-A10 are $\epsilon_{mn} = E_S$ and $\sigma_{mn} = 19.5 \text{ \AA}$, whereas for A7-A9 they are $\epsilon_{mn} = 0.01$ kcal/mol and $\sigma_{mn} = \sigma_U$.

Due to the choice $\epsilon_{mn} = 0.01$ kcal/mol, attraction between the beads interacting through a non-specific LJ potential is negligible in comparison with the thermal energy $k_B T \approx 0.6$ kcal/mol (k_B is the Boltzmann constant and $T = 300$ K is the temperature), so that the non-specific interactions do not drive the capsid conformation towards a wrong energy minimum. On the other hand, this choice still allows for the repulsion if two beads are too close to each other, accounting for the size of the protein pieces represented by the beads. Conversely, the specific LJ interactions mainly account for maintaining the appropriate capsid contacts.

The resulting model has two free parameters, the specific interaction energy E_S , which determines the strength of interaction between all beads for which a specific interaction is introduced, and the non-specific interaction radius σ_U , which describes the range of interaction between all beads which interact non-specifically. These parameters have been tuned in a series of SBCG simulations that sampled all permutations of $E_S = 5, 10, 20, 30,$ and 50 kcal/mol, and $\sigma_U = 8, 9, 10, 11,$ and 12 \AA . For each of the 25 simulations, we investigate the average radius of the capsid as a function of time and the radial mass distribution averaged over the last 100 ns at time $t = 4 \mu\text{s}$, as shown for several examples in Fig. S3. The parameters producing the results in best agreement with the native capsid structure are $\sigma_U = 10 \text{ \AA}$ and $E_S = 10 - 20$ kcal/mol. Checking also the maximal and minimal radii of the capsid, we conclude that $\sigma_U = 10 \text{ \AA}$ and $E_S = 10$ kcal/mol are the most suitable settings.

3 Supporting Results

3.1 Effect of the AFM pushing velocity on the FZ curve

In the SBCG simulations of AFM nanoindentation, the AFM tip is moved with a constant velocity, which is achieved through SMD by applying a force to the center of mass of the hemisphere that represents the tip. The forces observed in SMD simulations are typically orders of magnitude higher than those in the respective experiments, since the time scales of all-atom simulations are normally 10-100 ns, versus 0.1 s or longer for stretching/pushing experiments with biomolecules. With our SBCG model, the simulation time scale reaches $10 \mu\text{s}$, which is still much faster than the experiment, but the agreement between the simulated and experimental FZ curves suggests that such SMD velocity is already slow enough for an adequate comparison.

All simulations described in the main text are performed with the SMD velocity $v =$

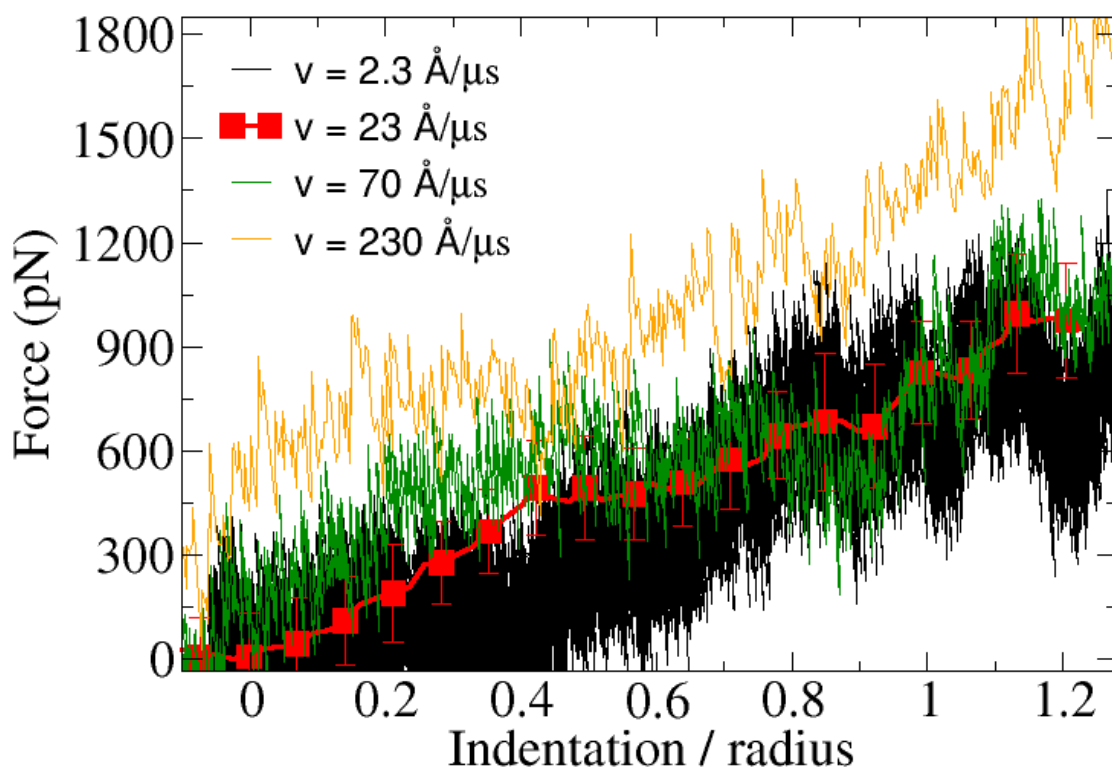


Figure S4: FZ curves for various velocities of the AFM tip in simulations. All curves are for pushing along the 5-fold symmetry axis of the HBV capsid. Red, average over five simulations with $v = 23 \text{ \AA}/\mu\text{s}$ (normal velocity used in simulations). Black, green, and orange curves are for individual simulations with varying velocities.

23 Å/μs, but additional simulations have been performed with SMD velocities varied from 2.3 Å/μs to 230 Å/μs. FZ curves for AFM nanoindentations of the HBV T=4 capsid are shown in Fig. S4. All simulations for which the results are shown have been performed with pushing along the 5-fold symmetry axis of the capsid. The average over five simulations with $v = 23 \text{ Å}/\mu\text{s}$ is shown in red. The simulation with a 10 times slower pushing, $v = 2.3 \text{ Å}/\mu\text{s}$, results in an FZ curve (black) that is close to that with $v = 23 \text{ Å}/\mu\text{s}$. Due to slower pushing, fluctuations are more prominent for the black curve than for individual simulations with $v = 23 \text{ Å}/\mu\text{s}$; FZ curves for all 15 individual simulations with $v = 23 \text{ Å}/\mu\text{s}$ are shown in Figs. S5 and S6.

A faster pushing with $v = 70 \text{ Å}/\mu\text{s}$ (green in Fig. S4) produces FZ curve that is slightly higher, but overall is in a close overlap with the $v = 23 \text{ Å}/\mu\text{s}$ curve (within the scatter of the curves for individual simulations with $v = 23 \text{ Å}/\mu\text{s}$). However, even faster pushing, $v = 230 \text{ Å}/\mu\text{s}$, results in the FZ curve (orange) that is noticeably above the $v = 23 \text{ Å}/\mu\text{s}$ curve. The curve follows approximately the same shape, but is shifted upwards by $\sim 300 \text{ pN}$, which occurs even before the AFM tip reaches the capsid. This additional force is due to the drag force from the solvent, which is represented implicitly using the Langevin equation (Eq. 3 in the main text). Indeed, the drag force experienced by an object of mass m_{tot} moving with a uniform velocity v is, according to the Langevin equation, $F_v = m_{tot}\gamma v$. The AFM tip consists of $\sim 2,000$ beads, each with the mass of 2 kDa, i.e., $m_{tot} \approx 4 \text{ MDa}$; $\gamma = 2 \text{ ps}^{-1}$, and $v = 230 \text{ Å}/\mu\text{s}$, which gives a drag force of $F_v \approx 300 \text{ pN}$. Three times slower pushing with $v = 70 \text{ Å}/\mu\text{s}$ corresponds to the drag force of $\sim 100 \text{ pN}$, which explains why the respective curve is somewhat higher than the one with $v = 23 \text{ Å}/\mu\text{s}$. For the velocity of $v = 23 \text{ Å}/\mu\text{s}$, commonly used in our simulations, the drag force is about 30 pN, which is significantly below the noise level in individual simulations.

Thus, simulations with a ten times slower pushing produces the FZ curve that is similar to those from simulations with $v = 23 \text{ Å}/\mu\text{s}$, and three times faster pushing also produces a similar FZ curve, while 10 times faster pushing leads to discrepancies. This finding shows that at $v = 23 \text{ Å}/\mu\text{s}$ the pushing reaches an adiabatic regime, i.e., it is unlikely that in the case of slower pushing the capsid exerts lower forces on the AFM tip. One extrapolates this conclusion to assume that the results of $v = 23 \text{ Å}/\mu\text{s}$ simulations apply to the experimental situation, where the AFM movement is $\sim 10,000$ times slower. Due to computational expense, we therefore choose $v = 23 \text{ Å}/\mu\text{s}$ (rather than smaller velocities) as a regular pushing velocity for the simulations that sample the AFM nanoindentations. We note that in the complete all-atom representation even slower pushing may be required to reach the adiabatic regime, due to the common effect of the CG modeling, namely, that relaxation processes are usually much faster in CG than in all-atom representation because of elimination of many degrees of freedom that contribute to friction.

3.2 Repeated pushing in individual simulations

FZ curves for three repeated rounds of AFM pushing in individual simulations, 15 such rounds for $Z_{max} = 0.35R$ and 15 for $Z_{max} = 1.25R$, are shown in Figs. S5 and S6 (c.f. FZ curves averaged over all simulations with pushing along one symmetry axis in Fig. 5 of the main text). Deformations of the capsid in each of these simulations, for the maximal indentation during the first round of pushing, as well as for the relaxation after the first round, are demonstrated in Figs. S7 and S8.

The results from individual simulations confirm the conclusion stated in the main text, that in simulations as well as in experiments, the FZ response of the HBV capsid is reversible if the indentation is stopped at $Z_{max} = 0.35R$ to $0.55R$, and is irreversible for larger indentations. Slight capsid deformations are observed for simulations with $Z_{max} = 0.35R$ even after the AFM is removed and the capsid relaxes, but the extent of this deformation is rather minor, so that the FZ curves corresponding to repeated pushing overlap with those for the first round within fluctuations. For $Z_{max} = 1.25R$, the FZ curves and snapshots from simulations show that after the first round the capsid remains deformed irreversibly. The FZ curves and snapshots for individual simulations also support the observation described in the main text, that capsid deformation and force response for indentations along the three different symmetry axes of the virus differ noticeably from each other.

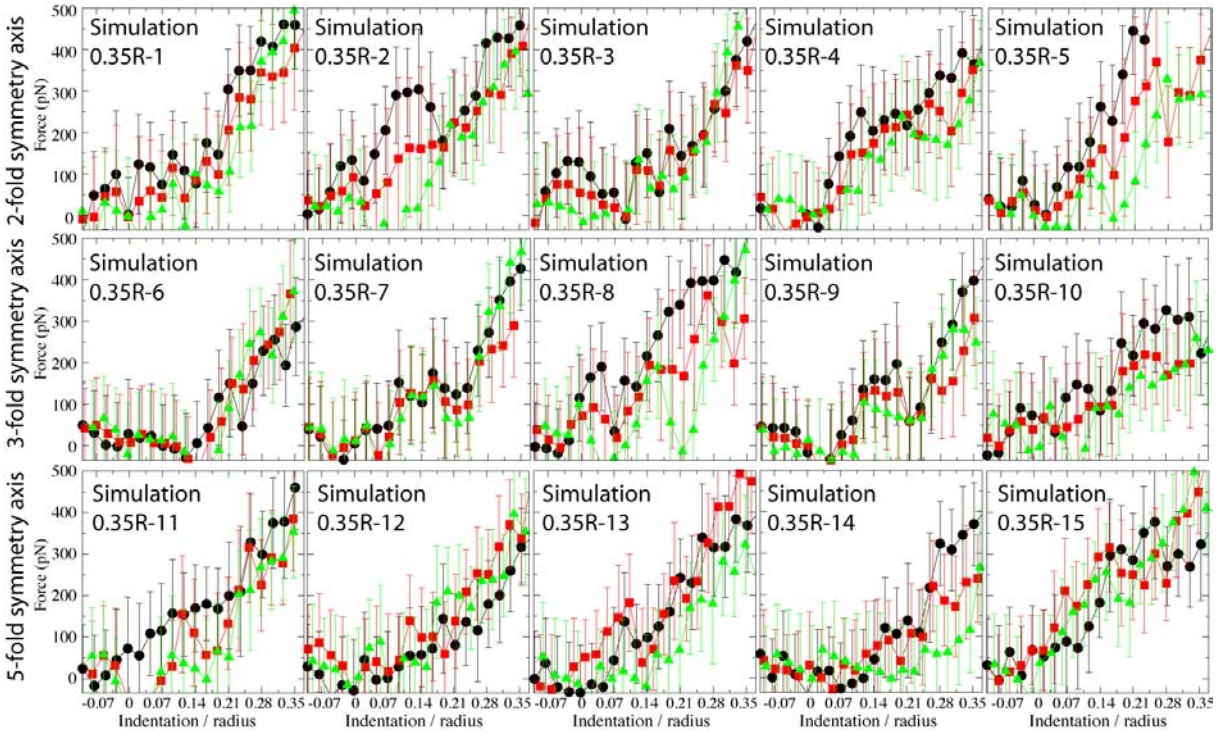


Figure S5: FZ curves in individual simulations with $Z_{max} = 0.35R$, for three rounds of repeated pushing. 1st round, black; 2nd round, red; 3rd round, green. The values are averaged over 150 ns time windows (the error bars are corresponding RMSDs).

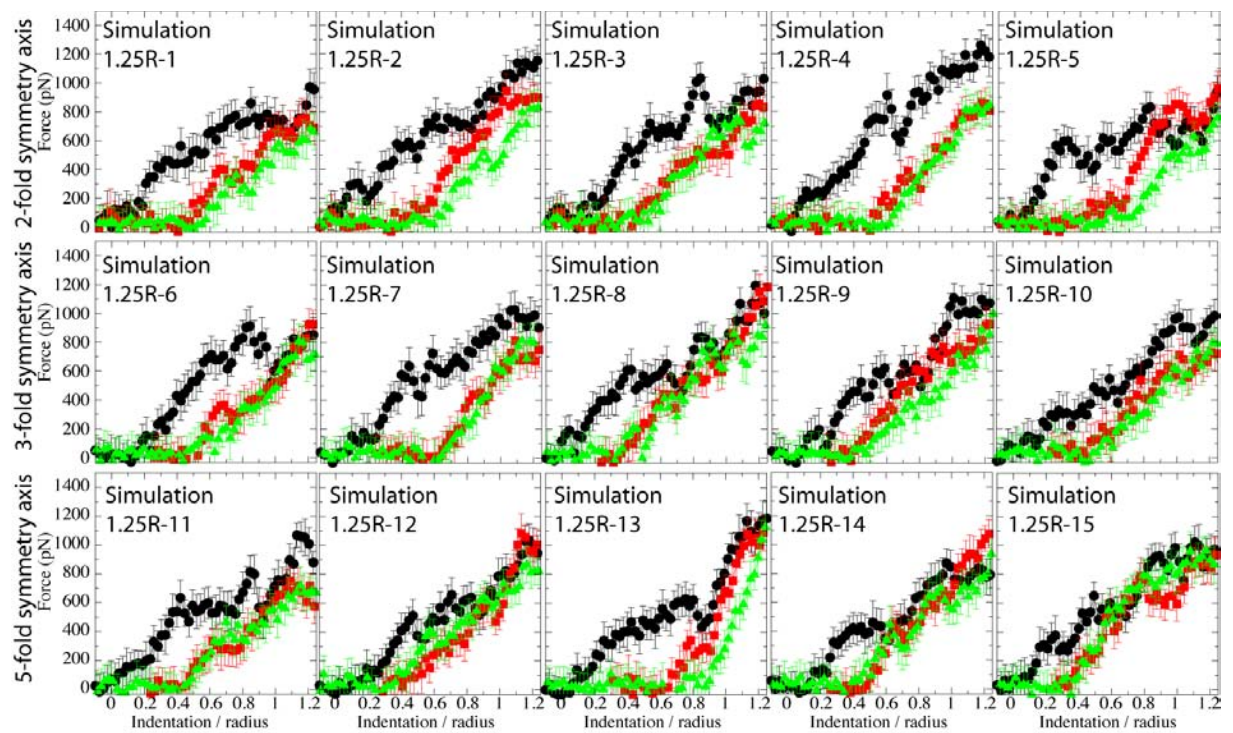


Figure S6: FZ curves in individual simulations with $Z_{max} = 1.25R$, for three rounds of repeated pushing. Colors and averaging are the same as in Fig. S5.

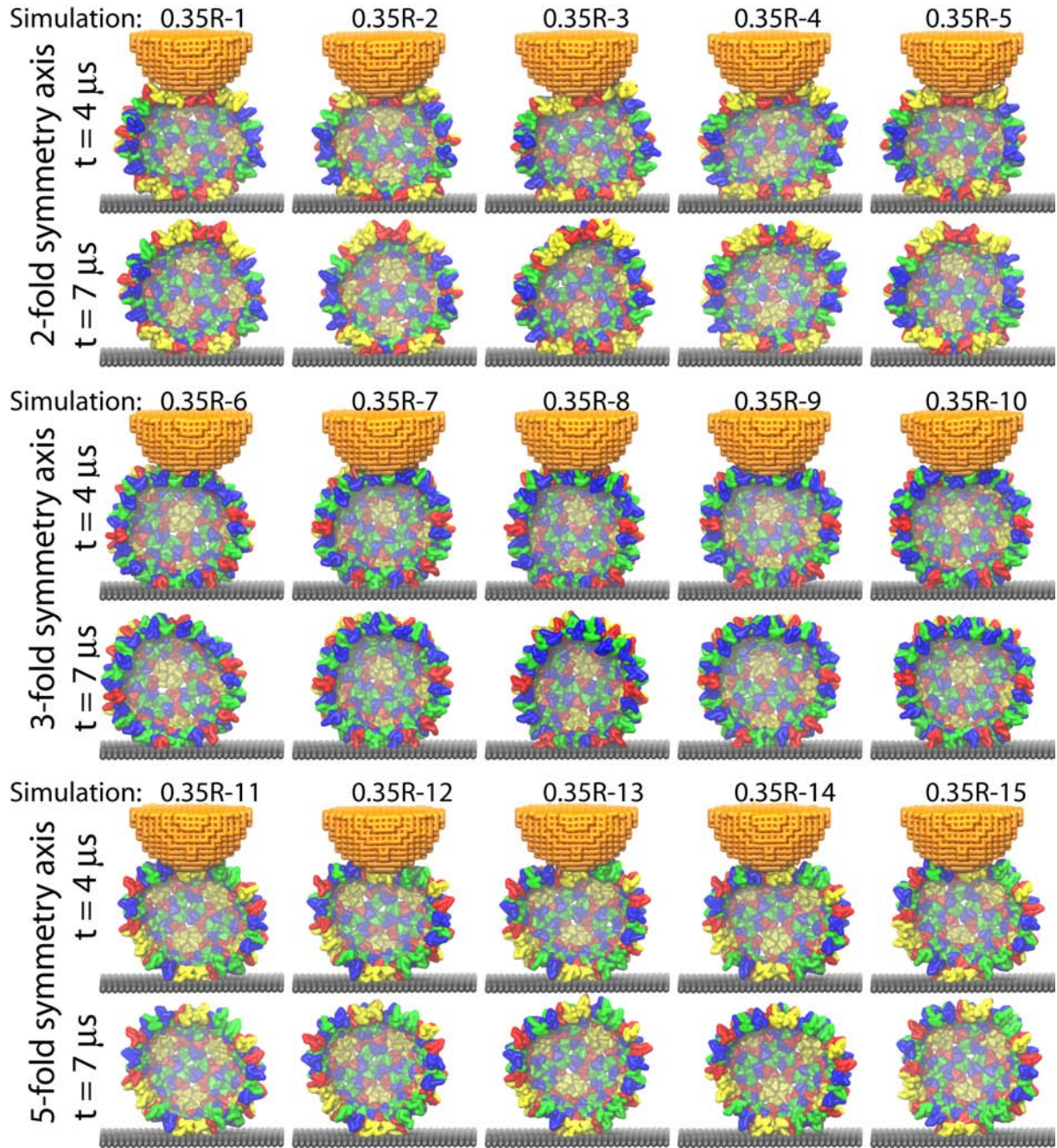


Figure S7: Deformation of the capsid in each of 15 individual simulations with $Z_{max} = 0.35R$. The capsid is shown at the time of the maximal indentation, $t = 4 \mu\text{s}$ (first round of pushing), and after the relaxation, $t = 7 \mu\text{s}$, which follows the first round of pushing as the AFM tip is retracted.

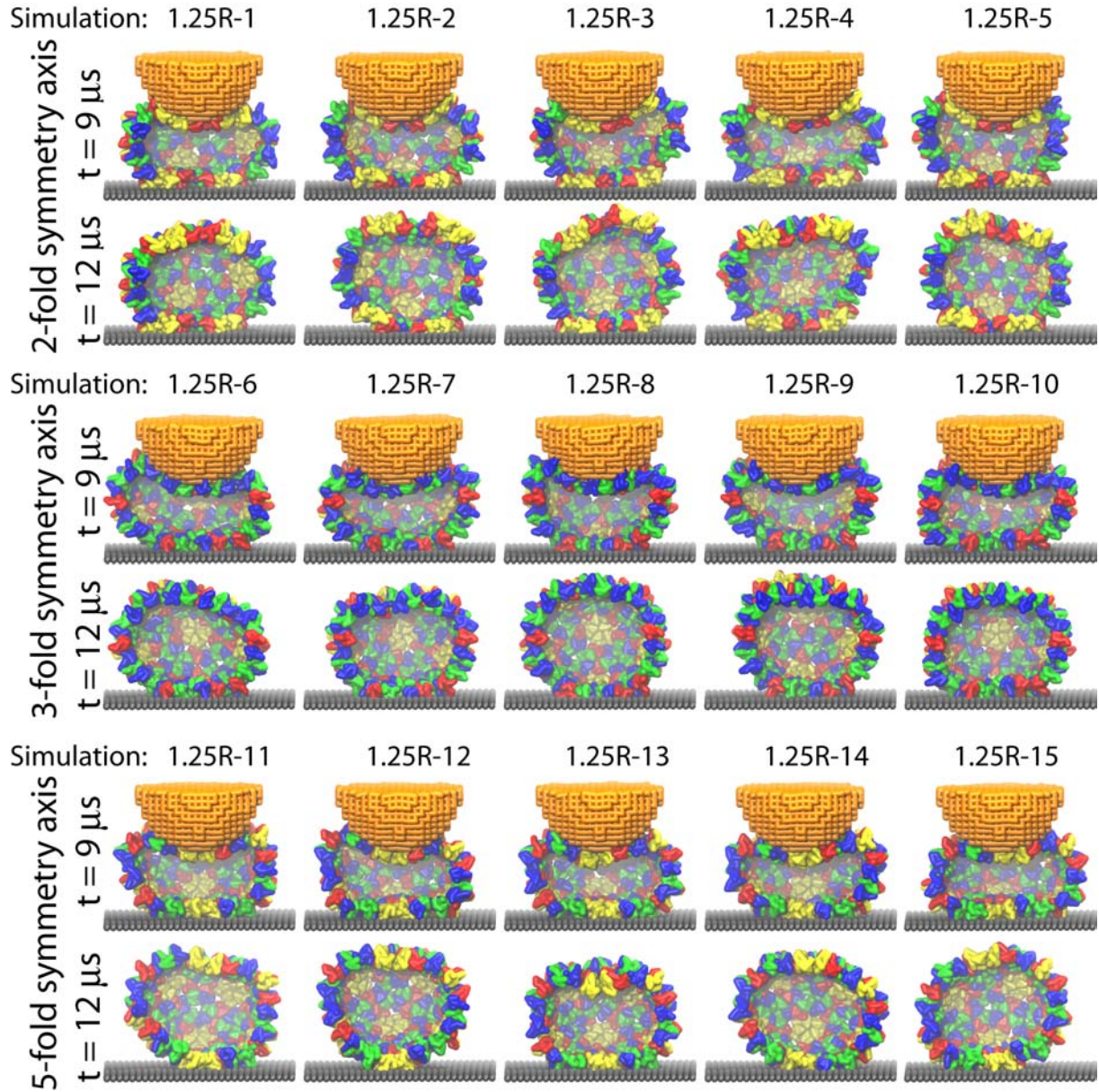


Figure S8: Deformation of the capsid in each of 15 individual simulations with $Z_{max} = 1.25R$. The capsid is shown at the time of the maximal indentation, $t = 9 \mu\text{s}$ (first round of pushing), and after the relaxation, $t = 14 \mu\text{s}$, which follows the first round of pushing as the AFM tip is retracted.

3.3 Capsid energies in simulations with $Z_{max} = 0.35R$

Fig. S9 shows the energies of bonded, angle, and nonbonded interactions within the capsid, as well as capsid-substrate interaction, for simulations with $Z_{max} = 0.35R$ (c.f. Fig. 6a of the main text, where the same values are shown for $Z_{max} = 1.25R$). After the first pushing round ($t > 4\mu s$), all energies analyzed remain relatively constant. Indeed, for $t > 4\mu s$ these energies fluctuate slightly around their average taken over $t > 4\mu s$, within the RMSD of the averaging, which is shown as a light blue shade around the deep blue line in Fig. S9. The average over $t > 4\mu s$ then gives a good measure of the level of the energies arising during all times for simulations with $Z_{max} = 0.35R$, in contrast with the $Z_{max} = 1.25R$ case, where some of the energies change significantly due to the capsid deformation. Thus, the average of the energies in the $Z_{max} = 0.35R$ case over $t > 4\mu s$ is used as a base line for the comparison with the $Z_{max} = 1.25R$ case in Fig. 3 of the main text.

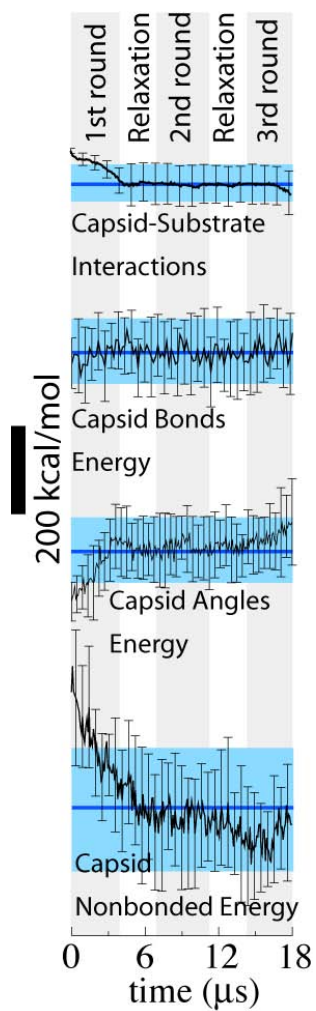


Figure S9: Energies for various interactions in the HBV-AFM system in simulations with $Z_{max} = 0.35R$. Black, average over all simulations with $Z_{max} = 0.35R$ (error bars are the averaging RMSDs). Blue, the average of the black curve over time $t > 4 \mu\text{s}$ (light blue shade, RMSD).

References

- [1] Arkhipov, A., P. L. Freddolino, and K. Schulten. 2006. Stability and dynamics of virus capsids described by coarse-grained modeling. *Structure*. 14:1767–1777.
- [2] Arkhipov, A., P. L. Freddolino, K. Imada, K. Namba, and K. Schulten. 2006. Coarse-grained molecular dynamics simulations of a rotating bacterial flagellum. *Biophys. J.* 91:4589–4597.
- [3] Arkhipov, A., Y. Yin, and K. Schulten. 2008. Four-scale description of membrane sculpting by BAR domains. *Biophys. J.* 95:2806–2821.
- [4] Yin, Y., A. Arkhipov, and K. Schulten. 2009. Simulations of membrane tubulation by lattices of amphiphysin N-BAR domains. *Structure*. 17:882–892.
- [5] Shih, A. Y., P. L. Freddolino, A. Arkhipov, and K. Schulten. 2007. Assembly of lipoprotein particles revealed by coarse-grained molecular dynamics simulations. *J. Struct. Biol.* 157:579–592.
- [6] Shih, A. Y., S. G. Sligar, and K. Schulten. 2008. Molecular models need to be tested: the case of a solar flares discoidal HDL model. *Biophys. J.* 94:L87–L89.
- [7] Marrink, S. J., A. H. de Vries, and A. E. Mark. 2004. Coarse grained model for semiquantitative lipid simulations. *J. Phys. Chem. B.* 108:750–760.
- [8] Marrink, S. J., H. J. Risselada, S. Yefimov, D. P. Tieleman, and A. H. de Vries. 2007. The martini forcefield: coarse grained model for biomolecular simulations. *J. Phys. Chem. B.* 111:7812–7824.
- [9] Wynne, S. A., R. A. Crowther, and A. G. W. Leslie. 1999. The crystal structure of the human hepatitis B virus capsid. *Mol. Cell.* 3:771–780.